Proceedings of the 5th International Conference on Fluid Flow and Thermal Science (ICFFTS 2024)
Lisbon, Portugal- November 21 - 23, 2024
Paper No. 164
DOI: 10.11159/icffts24.164

Numerical investigation of laminar forced convection through a dual orifice for shear-thinning fluids

Niharika Dutt[1], Tarak Monal[2], Swati A. Patel[3]
Department of Chemical Engineering, Indian Institute of Technology Ropar, Rupnagar Punjab-140001, India.
[1]niharika.20chz0012@iitrpr.ac.in, [2]tarakmondal@iitrpr.ac.in, [3]pswati@iitrpr.ac.in

Abstract - In this study, the two-dimensional laminar flow of shear-thinning fluids through a dual orifice in an isothermal pipe has been analysed numerically over a wide range of Reynolds number, $1 \leq Re \leq 100$, fixed orifice plate thickness, $\gamma = 1/16$ with the variation of diameter ratio of the orifice to pipe, $\beta = 0.2$ and 0.8 for a fixed orifice plate thickness, $\gamma = 1/16$. The numerical results have been derived for shear-thinning fluids over the range of power-law index, $0.2 \leq n \leq 1$ to analyse the flow kinematics and heat transfer characteristics. The flow field and heat transfer characteristics has been examined in terms of pressure coefficient, streamline patterns, velocity contours, centreline velocity and local Nusselt number over the range of diameter ratio of the orifice and the power-law index. The onset of vena contracta associated with the upstream orifice was found to be independent of the addition of the second orifice at the downstream but varies with orifice diameter ratio while the presence of vena contracta downstream of the second orifice was found to depend on the orifice diameter ratio. Also, the flow features downstream the second orifice is qualitatively like single orifice flow in terms of presence of recirculation, and reattachment but the flow features in the spacing between the two orifices are quite different having a donut-shaped vortex near the wall and jet-like flow in the core region. Also, the vortex formation lengthens as Reynolds number and power-law index increases for $Pr = 0.7$.

Keywords: Orifice meter, dual orifice, discharge coefficient, power-law fluids, shear-thinning fluids, Nusselt number.

1. Introduction

To manage flow rates and pressures, flow passage restrictions like control valves and orifices are used customarily in various engineering applications involving pipe systems. For industrial operations such as heating, ventilation and air conditioning control measures (HVAC), quality control in food processing industry, metering of highly viscous liquids, and calibrating instruments in metrology of liquid and gas flows, etc. accurate determination of flow characteristics through flow passage restrictions, especially orifices, is crucial [1]. In pre-mixed combustion, single orifice is frequently utilised to improve the homogeneity of flow distribution and the exchange of mass and heat, etc. [2,3].

The most popular kind of differential flowmeter for measuring single and multiphase flows is the orifice metre because of its straightforward construction, durability, and dependability. For the purposes of pressure control and/or flow rate control, orifices are also employed as flow limitation devices. Nevertheless, in addition to noise and vibration, the usage of orifices may cause significant erosion when solid particles are present, cavitation in liquid flows, choking in gas flows, and large hydraulic losses. Additionally, they are utilised with great care in pump recirculation lines to avoid cavitation and pump hunger [4,5]. In many applications, a single orifice cannot provide the necessary pressure drop without causing issues like liquid flashing, flow-choking in gas flows, or severe erosion from high flow velocities. In these situations, a multistage orifice can be utilised in the pipe let down line of power plant cooling systems and other process controls to accomplish the necessary pressure drop through the efficient arrangement of the orifices and optimal geometry design [6].

Numerous researchers have numerically and experimentally investigated the properties of orifice flow in detail while considering a variety of factors such as pipe diameter, intake velocity, orifice diameter, and orifice thickness. In order to establish correlations with the orifice geometry, the following significant flow properties are studied like velocity distribution, pressure distribution, discharge coefficients and heat transfer. The numerical analysis of orifice flow is getting attention in recent works [7,8] based on finite volume method [9-11]. Hollingshead, Johnson, Barfuss, and Spall [9] conducted a performance analysis using modelling and experimental measurements for four different types of differential pressure flowmeters like wedge, v-cone, standard concentric orifice, and venturi meter. Furthermore, most of the literature discusses the turbulent flow of Newtonian fluids, such as water, air, etc. The discharge coefficient is almost independent of *Re* in turbulent settings. Nonetheless, in the laminar regime met with viscous fluids, this connection is sensitive to *Re*, eccentricity

of the orifice, orifice thickness, etc. [11]. Consequently, the present work examines the laminar flow of viscous Newtonian and power-law fluids across a two-dimensional pipe for a dual orifice. Based on the review of the available literature, it is evident that there is a very little research done on the multistage orifice for non-Newtonian fluids. Furthermore, it is challenging for a practicing engineer to forecast the characteristics of pressure drop, liquid flashing, flow choking, and erosion due to the absence of set norms for such orifice arrangements. The difficulty in predicting the main flow features in multistage arises from the strong influence of the spacing between the orifices on the flow structure prevailing in between the orifices and downstream of the last orifice placed.

The present study considers the investigation of flow and heat transfer characteristics in a serial arrangement of two thin concentric edged orifices of different sizes placed with gaping between the orifices ($G = S/D$) i.e., $G = 2D/D = 2$ pipe by computational analysis, where S is the centre-to-centre distance between two orifices. Hence, this work investigates the laminar heat transfer flow from a dual orifice in shear-thinning fluids encompassing the range of parameters as Reynold number, $1 \leq Re \leq 100$, Prandtl number, $Pr = 0.7$, diameter ratio $\beta = 0.2$ and 0.8 and power-law index, $0.2 \leq n \leq 1$ for a fixed orifice plate thickness, $\gamma = 1/16$ in the steady-state regime. Furthermore, the effect of the order of the mounted orifices' diameter ratios, i.e., upstream $\beta = 0.2$, downstream $\beta = 0.8$ and downstream upstream $\beta = 0.8$, downstream $\beta = 0.2$ investigated in this work.

2. Problem formulation

The problem under consideration is the free stream of shear-thinning fluids flowing with velocity U and temperature T_c in an isothermal pipe (T_w) of diameter D approaching an orifice having an opening diameter d and thickness t as shown in Figure 1 maintained at temperature, T_w. The opening diameter and thickness of the orifice are the two geometrical parameters

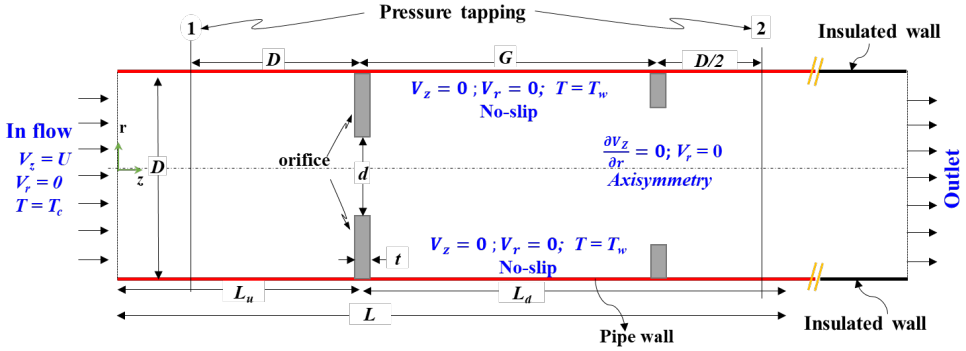

Figure 1: Schematic of the problem.

defined in their non-dimensional forms as β (= d/D) and, with fixed thickness, γ (= t/D), respectively. The shear-thinning fluid enters the pipe with a uniform velocity and constant temperature T_c ($< T_w$), having sufficient upstream length for flow to be fully hydraulically as well as thermally developed before approaching the orifice. The gap between the two orifice is defined as G (= S/D) = 2. Flow is considered to be two-dimensional and is expected to be steady and axisymmetric about the axis of the pipe for the range of geometric parameters, i.e. diameter ratio (β) and thickness of orifice (γ) over the range of Reynolds number (Re), and power-law index (n) for air ($Pr = 0.7$) in this study.

For steady, incompressible, and laminar flow, the continuity, momentum, and energy equations in their non-dimensional forms are written as follow:

Continuity equation:

$$\nabla \cdot V = 0 \tag{1}$$

Here, divergence of $V = 0$.

Momentum equation:

$$(V \cdot \nabla) V = -\nabla p + \frac{1}{Re} \nabla \cdot \tau \tag{2}$$

where, $-\nabla p$ = gradient of p, $\nabla \cdot \tau$ = divergence of tensor τ,

Energy equation:

$$(V \cdot \nabla)\theta = \frac{1}{Re\,Pr}\nabla^2\theta \tag{3}$$

The dependence of the deviatoric part of the stress tensor (τ) in the momentum equation, eq. (2) on the rate of deformation tensor $(\dot{\gamma})$ for power-law fluids (called constitutive equation) is expressed in the tensor form as:

$$\tau = m\left|\frac{1}{2}I_2\right|^{\frac{n-1}{2}}\dot{\gamma} \tag{4}$$

where, m and n are the fluid consistency coefficient and power-law index, respectively. The rate of strain tensor is defined as $\dot{\gamma} = \frac{1}{2}\left[(\nabla V) + (\nabla V)^T\right]$ and I_2 is strictly positive invariant given as $I_2 = \dot{\gamma} : \dot{\gamma} = \sum_i \sum_j \dot{\gamma}_{ij}^2$. The normalized form of equations (1)-(4) are owing to introducing non-dimensional variables as $V = \frac{V'}{U}$; $p = \frac{p'}{\rho U^2}$; $\nabla = D\nabla'$; $\eta = \frac{\eta'}{\eta_{ref}}$; $\eta_{ref} = m\left(\frac{U}{D}\right)^{n-1}$; $\tau = \frac{\tau'}{\eta_{ref}(U/D)}$; $\dot{\gamma} = \frac{\dot{\gamma}'}{(U/D)}$; $I_2 = \frac{I_2'}{(U/D)^2}$; $\theta = \frac{T_w - T}{T_w - T_m}$. Here, T_m is the bulk mean temperature at any section (z) defined as

$$T_m = \frac{\int_0^R V_r(r)T(r)r\,\mathrm{d}r}{\int_0^R V_r(r)r\,\mathrm{d}r} \tag{5}$$

The non-dimensional governing parameter for power-law fluids, Reynolds number, and Prandtl number, are defined as,

$$Re = \frac{\rho V^{2-n}D^n}{m},\quad Pr = \frac{mC_p}{k}\left(\frac{U}{D}\right)^{n-1}.$$

For axisymmetric flow assumed over the range of conditioned spanned in this problem, the physical realistic boundary conditions are given as:

- At the inlet of the pipe: $V_z = 1$, $V_r = 0$, $\theta = 0$.
- At the wall of the pipe: $V_z = V_r = 0$, $\theta = 1$.
- At the orifice surfaces: $V_z = V_r = \theta = 0$.
- At the exit of the pipe: $p = 0$; $\frac{\partial \varphi}{\partial z} = 0$, where $\varphi = V_z, V_r, \theta$.
- On the centerline axis: Symmetry about the axis of the pipe, $V_r = 0$; $\frac{\partial V_z}{\partial r} = \frac{\partial \theta}{\partial r} = 0$

The dimensionless static pressure differential ΔP^* is presented as $\Delta P^* = \frac{\Delta p}{\rho U^2}$, where ΔP is static pressure differential across the orifice and U is velocity at axis of the pipe. Here pressure difference has been taken from the computed axial static pressure values at the section D-D/2 upstream of the first orifice and downstream of the second orifice, respectively. The

pressure coefficient is defined as, $\left(\Delta p/\rho U^2\right)$. The average Nusselt number is defined as, $Nu = \frac{hD}{k}$, where h is the average heat transfer coefficient on the heated surface of the pipe and orifice.

3. Numerical Methodology:

Flow through a dual orifice in a pipe is solved using the finite element based commercial software COMSOL Multiphysics (Version 5.6). PARDISO scheme has been used in order to solve the set of continuity, momentum and energy equations (1)-(3) along with the aforementioned boundary conditions. The selection of numerical parameters (size of domain, and type and number of grid elements) is the crucial factor that influences the accuracy and reliability of the numerical scheme. Hence, domain independent test has been conducted by varying the domain length in upstream (L_u) and downstream (L_d) sections from the dual orifices at the extreme values of Reynolds number, Re = 1 and 100 for the order of mounting the orifices in the pipe β = 0.2 followed by β = 0.8 (case I) and, reverse order of the diameter ratio, i.e., β = 0.8 followed by β = 0.2 (case II). The results of pressure difference between the upstream and downstream sections of the dual orifices were measured for the upstream length (L_u) of 20D, and the downstream length (L_d) of 500D, 1000D, 1500D at n = 1 and 0.2.

The results of pressure difference confirm that the upstream length from the dual orifices, L_u = 20D in the present work for power-law index range, n = 1-0.2 while the downstream length, L_d = 500D for the range of n = 1-0.5 (Domain 1) and L_d = 1500D for n = 0.4-0.2 (Domain 2) were adequate and further increase in upstream and downstream lengths has not significant effect on the pressure difference due to dual orifices. The chosen upstream and downstream lengths have been scrutinized and confirmed for the flow to be hydrodynamically and thermally developed by examined the velocity and temperature profiles close to the upstream orifice and exit of the pipe. Furthermore, the grid independence test is performed at the extreme values of power-law index; n = 1 for Domain I and 0.2 for Domain II at Re = 100 as shown in Table 1 for the case I. The same grids are also tested for case II for the same set of parameters. The three non-uniform grids G1, G2 and G3 with the increasing level of refinement have been tested for both the cases. The grid used in this work is divided into two sub-regions. The sub-zone nearer to the orifice plate where the mesh is highly dense consists of quadrilateral elements while the region away from the orifice consists of quadrilateral elements coarse in nature as shown in Figure 2. Table 1 shows that as we move from G1 to G2 and G2 to G3 there is no significant difference observed in pressure difference values. This justifies that the chosen grids G2 having 337790 and 550292 elements in the computational domains, Domain I and II, respectively is sufficient to capture the

Table 1: Grid independence test for case I.

Grid	N_P	N_T	ΔP	N_P	N_T	ΔP
		n = 1			n = 0.2	
G1	60	308017	151.218	60	520035	197.924
G2	120	337790	148.708	120	550292	201.816
G3	180	367487	148.144	180	584599	201.674

steepest gradient in the dual orifices in a pipe flow. Figure 3 shows the radial velocity profiles at upstream (L_u = 20D, z/L = 0.034) and downstream (L_d = 500D and 1500D, z/L = 0.865 and 0.953) for n = 1 and 0.5; n = 0.4 and 0.2, respectively. Thus, this study was conducted using L_u = 20D (upstream), L_d = 500D and 1500D (downstream) and grid G2 = 337790 (Domain I) and 550292 (Domain II), respectively to examine the flow of shear-thinning fluid through orifice. The convergence criterion of 10^{-5} was set for momentum and thermal energy equations.

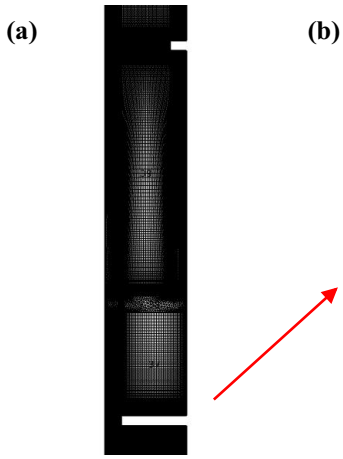

Figure 2: Grid structure of the **(a)** domain **(b)** expanded view near the orifice plate.

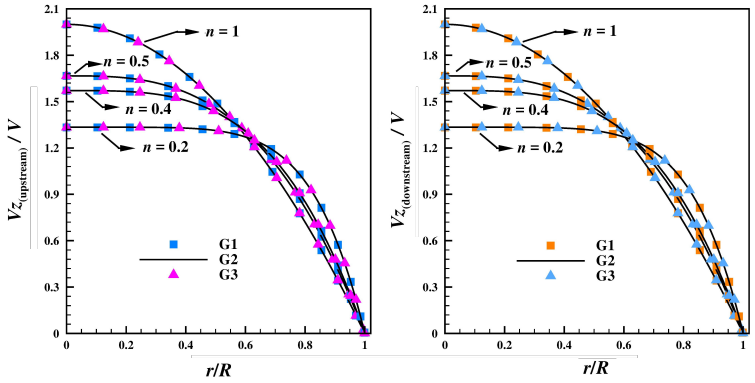

Figure 3: Radial velocity profiles at $Re = 100$, $Pr = 0.7$ for $n = 1$ and 0.5 at $L_u = 20$, $L_d = 500$ and for $n = 0.4$ and 0.2 at $L_u = 20$, $L_d = 1500$ at **(a)** upstream section **(b)** downstream section of the orifice.

4. Result and Discussion:

In this study, the effect of the order of the diameter ratio mounting in the pipe, i.e., $\beta = 0.2$ followed by 0.8 (case I) and $\beta = 0.8$ followed by 0.2 (case II) has been examined in the forced convection regime for a pipe through a square-edged orifices. The range of shear-thinning fluids ($0.2 \leq n \leq 1$) including Newtonian fluid as a limiting case has been considered in this study. The results are analysed in terms of the streamlines, velocity contours, the pressure difference, the centreline velocity, and the local Nusselt number. Before presenting the new results, the methodology has been validated by employing the available experimental and numerical findings in the literature for Newtonian fluids.

4.1 Validation

The previous results are compared with the present results for the limiting situations to determine the reliability of the chosen numerical method and precision of the new findings. Figure 4 exhibits the comparison of the present discharge

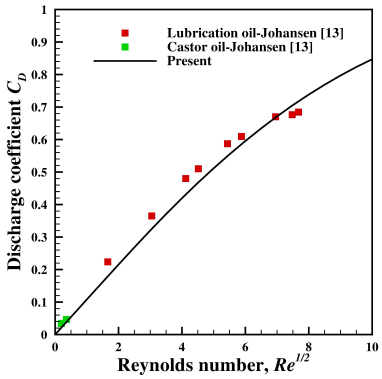

Figure 4: Comparison of discharge coefficient with respect to Reynolds number for $\beta = 0.8$, $\gamma = 1/16$, experimental Johansen [13] (symbols) and present (line) using orifice in a pipe.

Figure 5: Comparison of discharge coefficient with respect to Reynolds number for $\beta = 0.8$, $\gamma = 1/16$, numerically Sahin and Akilli [14] (symbols) and present (line) using orifice in a pipe.

coefficient for an orifice meter installed in a pipe with the experimental results by Johansen [13] that establishes good correspondence. Figure 5 validates the present discharge coefficient for an orifice meter using the experimental and numerical results by Sahin and Akilli [14]. Both the results are in close agreement with each other. Furthermore, qualitatively, Figure 6

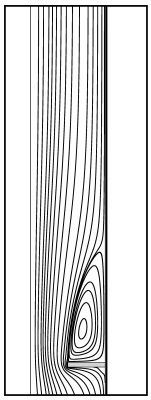

Figure 6: Comparison of streamlines at $Re = 40$, $\gamma = 1/16$, $\beta = 0.5$, $n = 1$ (Newtonian) Sahin and Ceyhan [15] (left); present (right).

compares the streamline patterns for the orifice plate with Sahin and Ceyhan [15] for $\gamma = 1/16$ $\beta = 0.5$ for $n = 1$ at Reynolds number, $Re = 40$. They seem to be in good agreement with each other. These comparisons are well aligned, giving rise to confidence in the chosen numerical scheme and the validity of the new data presented here.

4.2 Flow kinematics

The spatial variation of the velocity in the form of velocity contours around the orifice plate is customary to plot to understand the impact of power-law index and Reynolds number. Streamline patterns along with velocity contours are plotted for varying Reynolds number, and power-law index considered as shown in Figures 7 (a-c) for case I. It shows that for orifices with the diameter ratios, $\beta = 0.2$ followed by 0.8 vortex is formed only at the downstream attached to $\beta = 0.2$. The eye of the

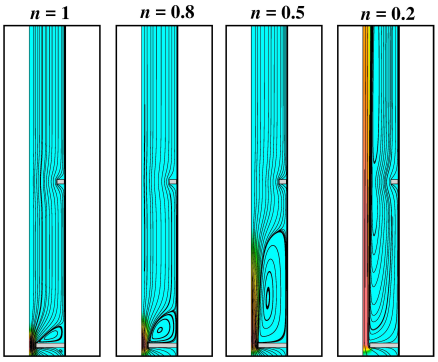

(a) **(b)** **(c)**

Figure 7: Streamline patterns for case I, $Pr = 0.7$ at **(a)** $Re = 1$ **(b)** $Re = 50$ **(c)** $Re = 100$ over the range of power-law index.

vortex is shifted away from the orifice $\beta = 0.2$ with the increase in Reynolds number for the fixed power-law index while similar trend has been observed for the decrease in power-law index at the fixed Reynolds number. On the other hand, as shown in Figures 8 (a-c) for the case II where orifice diameter ratio, $\beta = 0.8$ is followed by 0.2 for the flow separation observed

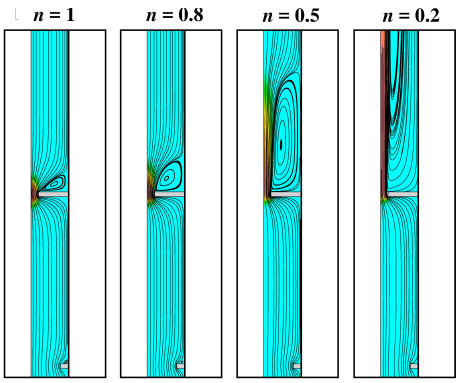

(a) **(b)** **(c)**

Figure 8: Streamline patterns for case II, Pr = 0.7 at **(a)** Re = 1 **(b)** Re = 50 **(c)** Re = 100 over the range of power-law index.

for both the orifices. The size of the vortices increases with the increasing Reynold number and decreasing power-law index. The velocity contours further confirm that the flow across orifice β = 0.2 experiences strong current due to the contraction of the flow area. In summary, as the Reynolds number and/or shear-thinning effect in the fluid increases the formation of vortices increases in size.

4.3 Centreline velocity and pressure coefficient

The nondimensional centreline velocity profiles have been plotted for case I and case II at Re = 100 over the range of power-law index in Figures 9 (a, b). The velocity profiles reveal that the highest magnitude of the centreline velocity is not much vary in either of the cases, in other words, β = 0.2 is mounted in any order in the pipe for constant G. Also, the location at which the centreline velocity approaches to unity is almost identical in both the cases in Figures 9 (a, b). Finally, the

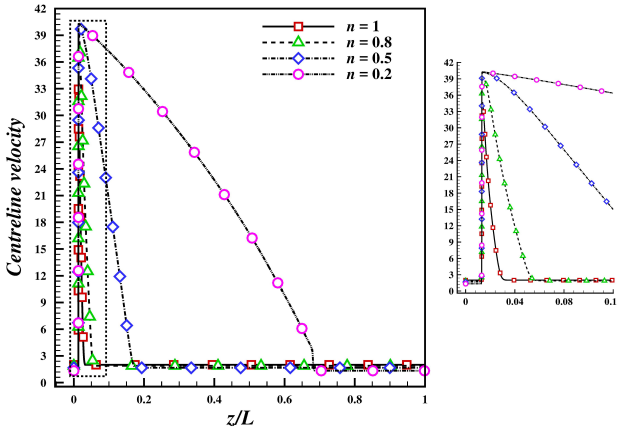

Figure 9 **(a)**: Centreline velocity for case I, Pr = 0.7 at Re = 100 over the range of power-law index.

Figure 9 **(b)**: Centreline velocity for case II, Pr = 0.7 at Re = 100 over the range of power-law index.

centreline velocity of the fluid with more shear-thinning properties delays in approaching the unity.

Also, the pressure coefficient as shown on Figure 10 (a, b) is the relative pressure in the flow field. It is clear from the pressure coefficient plots that the pressure coefficient decreases as the power-law index decreases. The pressure drop caused by the orifice results largely from the abrupt change in the flow passage in a pipe. This pressure drop can be estimated from the computed (or measured) static pressure variation by extrapolating the far upstream and far downstream linear pressure

variations towards the orifice plate. So, it is clear from the pressure distributions that there is only one location of minimum pressure with a magnitude depending on the orifice diameter ratio. Table 2 shows the difference in pressure from upstream

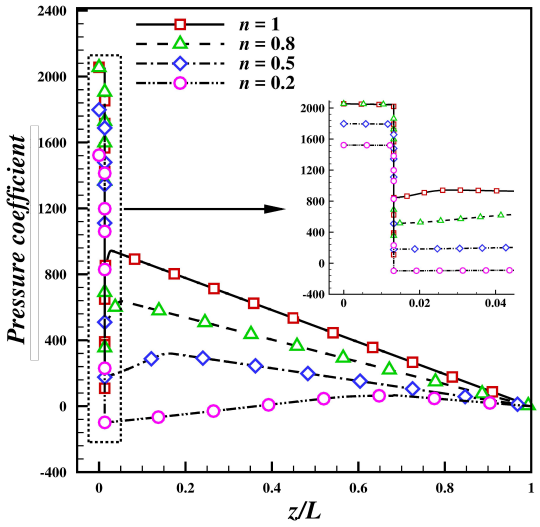

Figure 10 **(a):** Pressure coefficient for case I, Pr = 0.7 at Re = 100 over the range of power-law index.

Figure 10 **(b)**: Pressure coefficient for case II, Pr = 0.7 at Re = 100 over the range of power-law index.

and downstream section of the orifice for both cases of diameter ratio i.e. β = 0.2 followed by 0.8 and β = 0.8 followed by 0.2 at the extreme higher value of Reynolds number, Re = 100. The pressure drop is highest of n = 0.2 for either of the cases and it remains higher for case I in otherwise identical conditions except for Newtonian fluid (n = 1).

Table 2: ΔP values at Re = 100.

n	ΔP	
	Case I	**Case II**
1	148.69	153.99
0.8	191.34	188.42
0.6	200.65	194.66
0.5	201.39	195.19
0.4	201.80	195.42
0.3	201.96	195.48
0.2	201.81	195.43

4.4

Local Nusselt number

The Figure 11 shows typical distribution of local Nusselt number, Nu_L along the wall of the pipe for extreme Reynolds number, Re = 100 and n (0.2, 0.5, 0.8, 1) for case I. In general, Nu_L shows a complex trend in the vicinity of the orifice. For

away in the downstream section, Nu_L is seen to decrease to achieve its limiting values for thermally developed flow for all

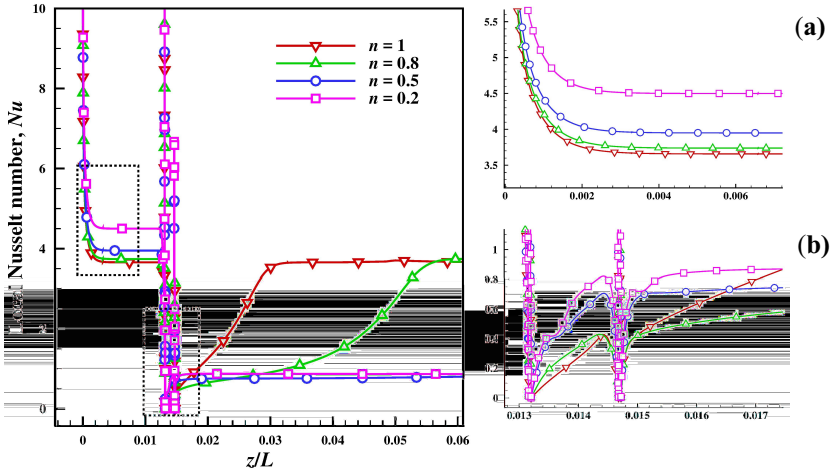

Figure 11: Local Nusselt number for case I, Pr = 0.7, Re = 100 over the range power-law index, **(a)** upstream of the orifice **(b)** downstream of the orifice.

the values of the power-law index considered as shown in Table 3. Figure 11 shows that the Newtonian fluid approaches the thermally developed flow quickly as compared to shear-thinning fluids. The increase in shear-thinning properties of the fluid delay the fluid to reach to the thermally developed flow.

Table 3: Nusselt number at Re = 100 at z/L = 0.08 (downstream of the orifice).

n	Nu
1	3.673
0.8	3.756
0.5	0.8443
0.2	0.8663

CONCLUSION

The range of parameters considered in this study are $1 \leq Re \leq 100$, $0.2 \leq n \leq 1$, $\beta = 0.2, 0.8$, $\gamma = 1/16$ (constant) for air as a process fluid. The detailed analysis of streamlines, pressure coefficient, centreline velocity, pressure difference, local Nusselt number is shown for the two different assembly of the dual orifices mounted in the pipe with diameter ration, $\beta = 0.2$ followed by 0.8, and $\beta = 0.8$ followed by 0.2. The streamline patterns are shown for the varying Reynolds number, and it is influenced by the diameter ratio and power-law index values strongly over the range of Reynolds number. The pressure difference from upstream and downstream section of the orifice increases as the effect of shear-thinning decreases for the combination of the diameter ratio for higher Reynolds number. The decrease in power-law index at fixed Reynolds number delays the flow to approach the thermally developed flow condition.

NOMENCLATURE

C_p	Heat capacity	[J/K]
d	Diameter of the orifice	[m]
D	Diameter of the pipe	[m]
G	Gap between the two orifices (= S/D)	[m]
k	Thermal conductivity of the fluid	[W/mK]
L	Total length of the pipe	[m]

n	Power-law index	--
Nu_L	Nusselt number	--
ΔP^*	Static pressure difference	[Pa]
r	Radial coordinate	--
Re	Reynolds number	--
S	Distance between the orifice	[m]
t	Thickness of the orifice	[m]
T_C	Inlet temperature	[K]
T_m	Bulk mean temperature	[K]
T_w	Wall temperature	[K]
U	Inlet velocity of the fluid	[m/s]
U_{max}	Maximum velocity	[m/s]
V_z	Dimensionless velocity in z-direction	[m/s]
V_r	Dimensionless velocity in r-direction	[m/s]
z	Axial coordinate	--
Greek symbol		
$\beta = d/D$	Diameter ratio	--
$\gamma = t/d$	Thickness-to-diameter ratio	--
σ	Cauchy stress tensor	[Pa]
μ	Viscosity of the fluid	[N s/m^2]
ρ	Density of the fluid	[kg/m^3]
τ	Devioteric part of Cauchy stress tensor	[Pa]
θ	Non-dimensional temperature	--

REFERENCES

[1] T. Gronych, M. Jerab, L. Peksa, J. Wild, F. Stanek, M. Vicar, "Experimental study of gas flow through a multi-opening orifice,". *Vacuum* 86 (11), pp. 1759–1763, 2012.

[2] M.K. Roul, S.K. Dash, "Single-phase and two-phase flow through thin and thick orifices in horizontal pipes," *J. Fluids Eng.* 134 (9), 91301, 2012.

[3] A.A. Araoye, H.M. Badr, W.H. Ahmed, "Investigation of flow through multi-stage restricting orifices," *Annals of Nuclear Energy*, vol. 104, pp. 75–90, 2017.

[4] W. Haimin, X. Shujuan, S. Qingyi, Z. Caimin, L. Hao, C. Eryun, "Experimental study on pressure drop of a multistage letdown orifice tube," *Nucl. Eng. Des*. vol. 265, pp. 633–638, 2013.

[5] H.P. Rani, T. Divya, R.R. Sahaya, V. Kain, D.K. Barua, "Numerical investigation of energy and Reynolds stress distribution for a turbulent flow in an orifice," *Eng. Fail. Anal*. vol. 34, pp. 451–463, 2013.

[6] W. Haimin, X. Shujuan, S. Qingyi, Z. Caimin, L. Hao, C. Eryun, "Experimental study on pressure drop of a multistage letdown orifice tube," *Nucl. Eng. Des*. vol. 265, pp. 633–638, 2013.

[7] V.K. Singh, T.T. John Tharakan, "Numerical simulations for multi-hole orifice flow meter," *Flow Meas. Instrum*. vol. 45, pp. 375–383, 2015.

[8] M.S. Shah, J.B. Joshi, A.S. Kalsi, C.S.R. Prasad, D.S. Shukla, "Analysis of flow through an orifice meter: CFD simulation," *Chem. Eng. Sci*. vol. 71, pp. 300–309, 2012.

[9] C.L. Hollingshead, M.C. Johnson, S.L. Barfuss, R.E. Spall, "Discharge coefficient performance of Venturi, standard concentric orifice plate, V-cone and wedge flow meters at low Reynolds numbers," *J. Pet. Sci. Eng*. vol. 78 (3–4), pp. 559–566, 2011.

[10] R.D. Mills, "Numerical solutions of viscous flow through a pipe orifice at low Reynolds numbers," *J. Mech. Eng. Sci*. vol. 10 (2), pp. 1–9, 1968.

[11] N. Arun, S. Malavarayan, M. Kaushik, "CFD analysis on discharge co-efficient during non-Newtonian flows through orifice meter," *Int. J. Eng. Sci. Technol*. vol. 2 (7), pp. 3151–3164, 2010.